Mon. Not. R. Astron. Soc. **000**, 1–12 (2011) Printed 12 January 2013 (MN LATEX style file v2.2)

The star formation history of the Large Magellanic Cloud star cluster NGC 1751 ⋆

Stefano Rubele[1,2], Léo Girardi[1], Vera Kozhurina-Platais[3], Paul Goudfrooij[3], Leandro Kerber[4]

[1] *Osservatorio Astronomico di Padova – INAF, Vicolo dell'Osservatorio 5, I-35122 Padova, Italy*
[2] *Dipartimento di Astronomia, Università di Padova, Vicolo dell'Osservatorio 2, I-35122 Padova, Italy*
[3] *Space Telescope Science Institute, San Martin Drive, Baltimore, USA*
[4] *Universidade Estadual de Santa Cruz, Rodovia Ilhéus-Itabuna, km. 16 – 45662-000 Ilhéus, Bahia, Brazil*

arXiv:1102.2814v1 [astro-ph.SR] 14 Feb 2011

To appear in MNRAS

ABSTRACT

The HST/ACS colour–magnitude diagrams (CMD) of the populous LMC star cluster NGC 1751 present both a broad main sequence turn-off and a dual clump of red giants. We show that the latter feature is real and associate it to the first appearance of electron-degeneracy in the H-exhausted cores of the cluster stars. We then apply to the NGC 1751 data the classical method of star formation history (SFH) recovery via CMD reconstruction, for different radii corresponding to the cluster centre, the cluster outskirts, and the underlying LMC field. The mean SFH derived from the LMC field is taken into account during the stage of SFH-recovery in the cluster regions, in a novel approach which is shown to significantly improve the quality of the SFH results. For the cluster centre, we find a best-fitting solution corresponding to prolonged star formation for a for a timespan of 460 Myr, instead of the two peaks separated by 200 Myr favoured by a previous work based on isochrone fitting. Remarkably, our global best-fitting solution provides an excellent fit to the data – with χ^2 and residuals close to the theoretical minimum – reproducing all the CMD features including the dual red clump. The results for a larger ring region around the centre indicate even longer star formation, but in this case the results are of lower quality, probably because of the differential extinction detected in the area. Therefore, the presence of age gradients in NGC1751 could not be probed. Together with our previous findings for the SMC cluster NGC 419, the present results for the NGC 1751 centre argue in favour of multiple star formation episodes (or continued star formation) being at the origin of the multiple main sequence turn-offs in Magellanic Cloud clusters with ages around 1.5 Gyr.

Key words: Stars: evolution – Hertzsprung-Russell (HR) and C-M diagrams

1 INTRODUCTION

A few stars clusters in the Magellanic Clouds present in their CMDs, in addition to multiple main sequence turn-offs (MMSTO; Mackey & Broby Nielsen 2007; Mackey et al. 2008; Milone et al. 2009; Goudfrooij et al. 2009; Glatt et al. 2008), also dual red clumps (Piatti et al. 1999; Girardi et al. 2009). The MMSTO features can be interpreted either as the presence of different generations of stars spanning several 10^8 yr in these clusters (Mackey & Broby Nielsen 2007; Mackey et al. 2008; Milone et al. 2009; Goudfrooij et al. 2009), or as the manifestation of some other effect intrinsic to coeval stars such as a dispersion in rotational velocities (Bastian & de Mink 2009, see however Girardi, Eggenberger, & Miglio 2011). However, the simultaneous presence of a dual red clump feature favours the former interpretation (Girardi et al. 2009; Rubele et al. 2010): it indicates a modest spread in the core mass of stars leaving the main sequence which is well compatible with the age spread of a few 10^8 yr deduced from the shape of the MMSTOs.

The SMC star cluster NGC 419 is presently the most

⋆ Based on observations with the NASA/ESA *Hubble Space Telescope*, obtained at the Space Telescope Science Institute, which is operated by the Association of Universities for Research in Astronomy, Inc., under NASA contract NAS5-26555

striking example of a cluster containing a dual red clump. Rubele et al. (2010) demonstrated that the assumption of an extended star formation history (SFH) in NGC 419, explored by means of the classical method of SFH-recovery via CMD-reconstruction, produces indeed a remarkably good quantitative description of the observed CMDs. The SFH was found to extend over a period of 700 Myr. The same analysis has produced quite stringent limits to the cluster's distance, reddening, and metallicity.

Although not explicitly discussed by Rubele et al. (2010), the dual red clump of NGC 419 has played an important role in limiting the family of stellar models that could be fit in the process of CMD-reconstruction, because dual red clumps can only happen within a relatively narrow interval of ages. In this paper, we examine the case of the LMC star cluster NGC 1751, which as noted by Girardi et al. (2009), does also appear to present a dual red clump, and hence should be a good target for the CMD-reconstruction technique. We will use the extremely accurate data available from HST/ACS, and analyses techniques similar to those applied by Girardi et al. (2009) and Rubele et al. (2010) for deriving the SFH. Sect 2 will briefly present the data and discuss the reality of the dual red clump. The next sections will present the SFH-recovery method and its application to the NGC 1751 surrounding LMC field (Sect. 3) and cluster area (Sect. 4). Sect. 5 draws the final conclusions.

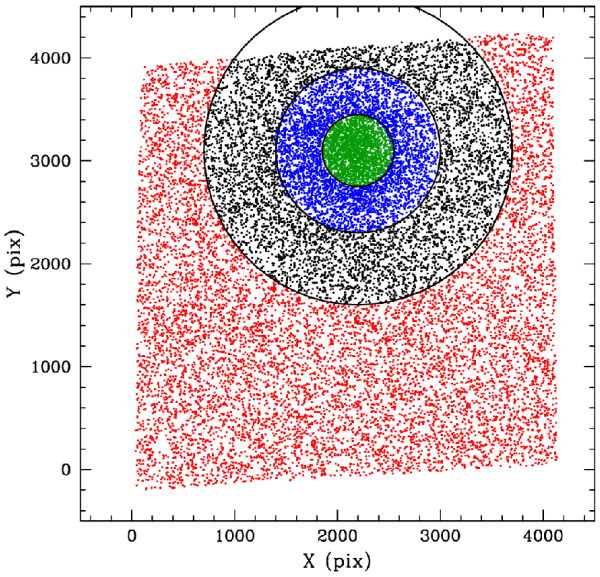


Figure 1. Map of the stars used in this work, in the xy plane of the ACS/WFC images. The scale is of about 0.05 arcsec/pix. The observed stars have been grouped in areas corresponding to the LMC field (red) and, for NGC 1751, an inner "Centre" (green) and outer "Ring" (blue).

2 THE NGC 1751 DATA AND ITS DUAL RED CLUMP

2.1 Data and photometry

The dataset used in this paper comes from GO-10595 (PI: Goudfrooij), and consists of one short and two long exposures in F435W, F814W, and F555W with small dither pattern to avoid the ACS/WFC gap between two WFC chips. A detailed description of the observations and photometry is given in Goudfrooij et al. (2009). Nevertheless, in this paper we use the simultaneous ePSF fitting technique as it described in Anderson et.al. (2008), which fits the PSF simultaneously on all exposures/observations of the cluster. Differently from Goudfrooij et al. (2009), the Charge Transfer Efficiency (CTE) correction was performed using Riess & Mack (2004) formula (ACS-ISR 2005). The derived photometry was calibrated into the Vegamag system as described in Goudfrooij et al. (2009).

Fig. 1 shows a spatial representation of the stars we analize in this work. We have initially located the center of NGC 1751 at the position $x_c = 2200$ pix, $y_c = 3100$ pix. Based on the appearance of the CMDs at varying radii r from this center, we have defined regions of the ACS/WFC images corresponding to

- the LMC **Field**, for $r > 1500$ pix (73.5 arcsec);
- the main body of the NGC 1751 cluster, for $r < 800$ pix (39.2 arcsec), which is further divided into:
 - the **Centre**, for $r < 350$ pix (17.2 arcsec);
 - the **Ring**, for $350 < r < 800$ pix ($17.2 < r < 39.2$ arcsec).

These regions are depicted in Fig. 1. The Centre, Ring and Field regions have areas of 0.385, 1.63, and 10.30 pix^2 (5.3, 22.6, 143 arcmin^2), respectively. Figure 2 shows how the stellar density varies as a function of radius from the NGC 1751 centre, taking into account only the stars of $F814W < 22$, for which the photometry should be close to complete. The figure clearly shows the flattening of the density for $r > 1500$ pix, which indicates that indeed that is a good choice for defining the LMC Field.

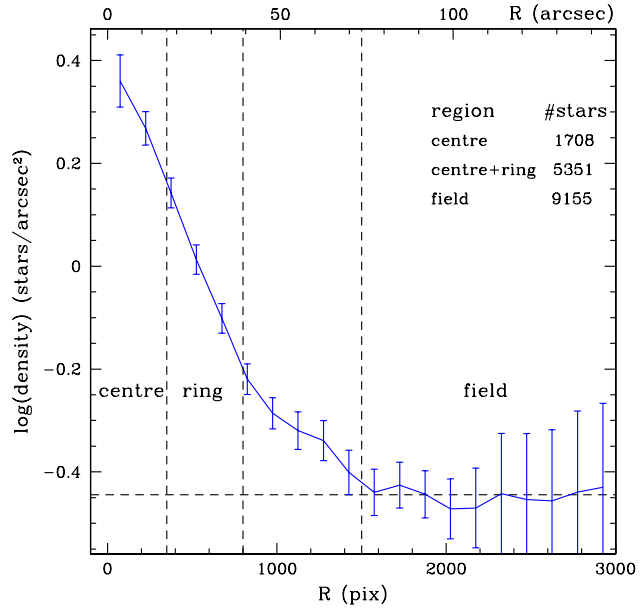


Figure 2. The logarithm of stellar density as a function of radius from the NGC 1751 centre. Error bars are the random errors.

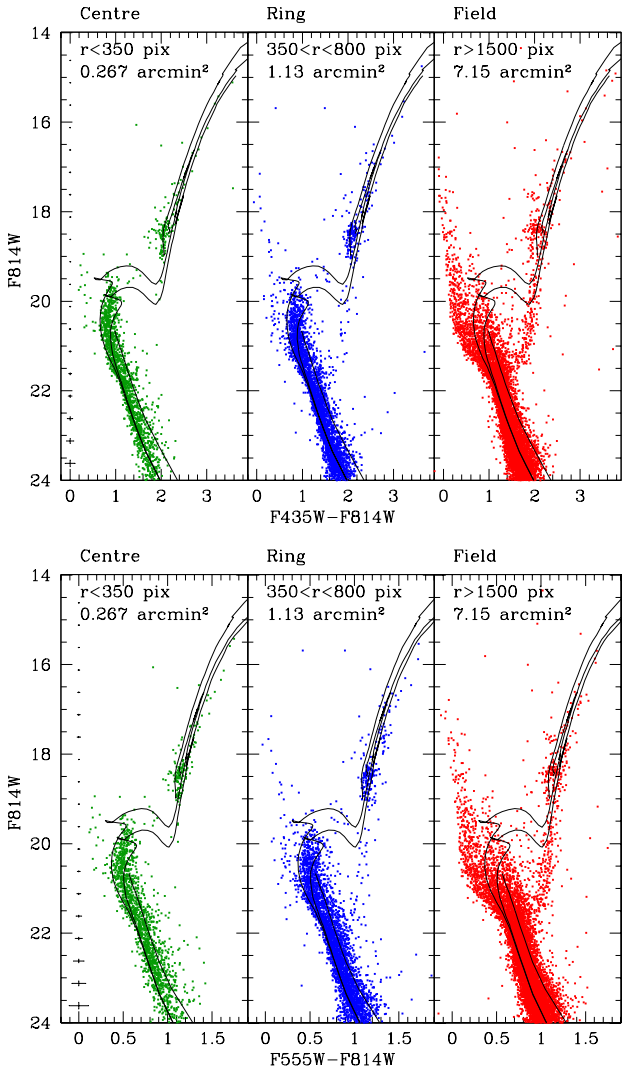


Figure 3. The CMDs for NGC 1751 as derived from the ACS/WFC data, using both $F435W - F814W$ (top panels) and $F435W - F814W$ (bottom panels) colours versus the $F814W$ magnitude. Panels from left to right present data for the cluster Centre and Ring, and LMC Field. As a reference to the eye, the panels also show the position of 1.12 and 1.42-Gyr isochrones of metal content $Z = 0.008$, shifted by $(m-M)_0 = 18.50$ and $A_V = 0.7$, together with the expected location of equal-mass binaries along the main sequence (continuous lines). The tiny crosses at the leftmost extreme of the left panel are 1σ error bars derived from artificial star tests in the cluster Centre (see Sect. 2.2). The error bars for the Ring and Field are not shown in the figure; they are of about the same size for the brightest magnitudes, becoming just ~ 25 % smaller for the faintest magnitudes.

In this work, we will analyse both the Centre and Ring regions, which present a good density contrast with respect to the field. Although the cluster clearly extends up to a radius of 1500 pix, the region with $800 < r < 1500$ pix will not be considered further.

Fig. 3 shows the ACS data for the different regions of NGC 1751, in the F814W vs. F435W − F814W and F814W vs. F555W − F814W CMDs. These plots will be used as a reference in our analysis.

The CMDs for the cluster Centre show very clearly the broad main sequence turn-off of this cluster, its dual red clump, and other well-known CMD features such as the sequence of binaries parallel to the main sequence, and the RGB, subgiants, and early-AGB bump. A simple comparison between the CMDs for the Centre and Field reveals that the field contamination in the cluster central regions is close to negligible. This is clear already looking at the star counts in the red clump: the 7.15 arcmin^2 of Field contain 189 red clump stars (here defined as stars with $18.05 < F814W < 19.15$, $F435W - F814W > 1.5$), therefore the 0.267 arcmin^2 of the Centre are expected to contain just ~ 7 red clump stars coming from the LMC field, which is far less than necessary to explain any of the features of its CMD. Indeed, the red clump in the Centre is made of 117 stars, which can be separated into the 89 "bright" ones ($F814W < 18.75$) – which correspond to the classical red clump made of stars which likely passed through electron degeneracy in their cores – and 28 faint or "secondary" ones ($F814W > 18.75$) – which were likely able to avoid it. We can conclude, in a way similar to the case of NGC 419 (Girardi et al. 2009, 2010), that the probability that the dual red clump observed in the centre of NGC 1751 is caused by LMC field stars is less than $P \sim 5 \times 10^{-6}$, and therefore negligible.

Note that differences are quite evident in the position of CMD features between the Centre and Field, which are obviously mixed in the CMD of the Ring. The Field presents an old main sequence turn-off and subgiant sequence extending to magnitudes as faint as $F814W < 21.5$, and a younger main sequence extending as bright as $F814W < 16.5$. Just traces of these features are present in the CMD of the Centre. Moreover, the red clump in the Field do also present a composite structure, with a ratio of faint/bright stars of 59/130. This latter feature is just expected from a field made of stars covering a wide range of ages and initial masses (see Girardi 1999; Piatti et al. 1999), and being observed with very small photometric errors as in this case.

2.2 Assessing photometric errors and completeness

In order to characterize the errors in the photometry and the completeness of the sample, we have performed a series of artificial star tests (AST) on the reduced images (see e.g. Gallart et al. 1999; Harris & Zaritsky 2001).

The procedure consists of adding stars of known magnitude and colour at random places in each exposure, and redoing the photometry exactly in the same way as described in Sect. 2.1. The artificial stars are considered to be recovered if the input and output positions are closer than 0.5 pixels, and flux differences are less than 0.5 mag.

In order to avoid the introduction of additional crowding in the images, artificial stars are positioned at distances much higher than their PSF width. So, our AST are distributed on a grid spaced by 20 pix, which is each time randomly displaced over each set of exposures.

A total of 1.04×10^7 ASTs were performed, covering in an almost uniform way the CMD area of the observed stars as well as the area for which we build the "partial models" to be used in the SFH analysis (see Sect. 4.2 below). Then, the ratio between recovered and input stars gives origin to the completeness map of Fig. 4. Note that the 90 % completeness

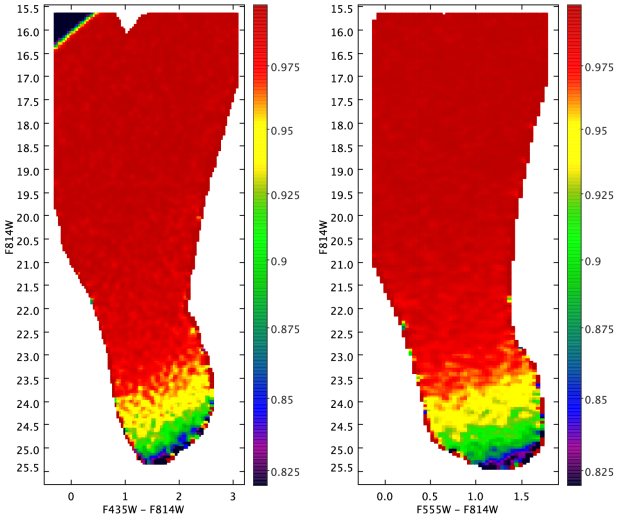


Figure 4. Completeness map, derived from the complete set of ASTs realised over NGC 1751 (centre plus ring areas), for both the F814W vs. F435W − F814W (left panel) and F814W vs. F555W − F814W (right panel).

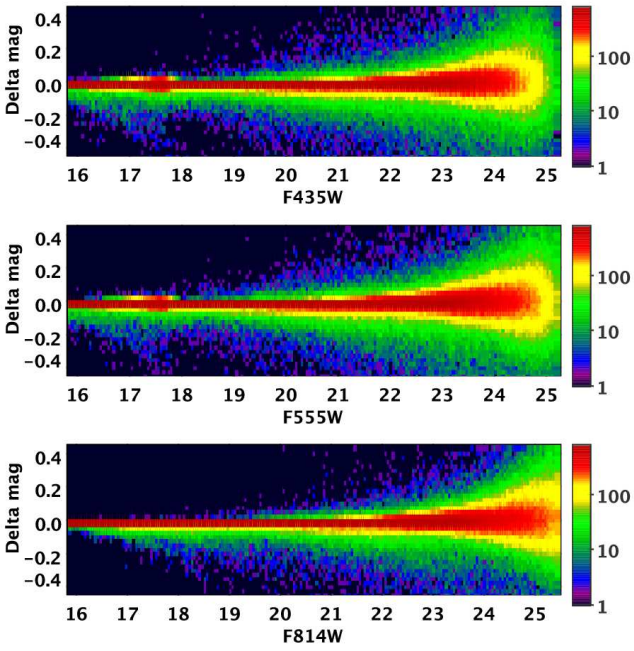


Figure 5. Map of photometric errors as a function of input F435W, F555W and F814W (from top to bottom), as derived from the ASTs over the core of the cluster area (that is, in the Centre plus Ring). The errors are defined as the difference between the recovered and input magnitudes.

limit is located at F814W $\sim$ 24.5, which is well below the position of the MMSTOs in NGC 1751.

Figure 5 illustrates the differences between the recovered and input magnitudes of the ASTs, as a function of their input magnitudes. These differences give a good handle of the photometric errors effectively present in the data. The error distributions are slightly asymmetric because of crowding.

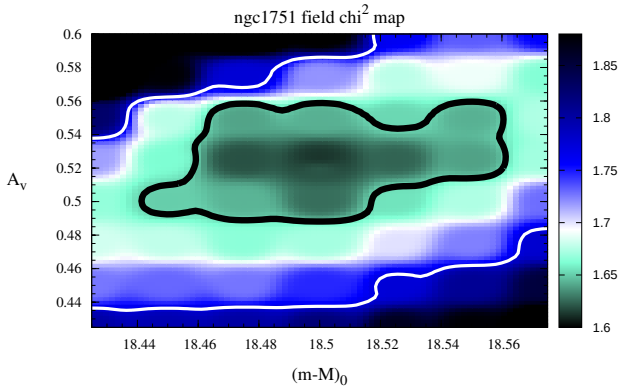


Figure 6. χ^2 map for the Field best-fitting solution, as a function of distance modulus and V-band extinction. The continuous lines show the 68 % (black) and 95 % (white) confidence levels for the overall best-fitting solution, which is located at $(m-M)_0 = 18.50$, $A_V = 0.525$.

3 THE SFH OF THE LMC FIELD

3.1 Overview of the method

To recover the SFH from the ACS data, we use the pipeline built to analyse data from the VISTA survey of the Magellanic Clouds (VMC; see Cioni et al. 2011). The method has been fully described and tested by Kerber et al. (2009) using simulated near-infrared data, and by Rubele et al. (2010) using ACS/HRC data for the SMC cluster NGC 419. The method consists in (1) building the Hess diagram for the data and a series of "partial models" which represent populations in limited intervals of age and metallicity, and (2) using the StarFISH code (Harris & Zaritsky 2001, 2004) to find the linear combination of partial models that minimizes a χ^2-like statistic as defined in Dolphin (2002). The solution is characterized by the minimum χ^2, $\chi^2_{\rm min}$, and by a set of partial model coefficients corresponding to the several age bins. These latter translate directly into the star formation rate as function of age, SFR(t).

The age–metallicity space occupied by the partial models depends on the object under consideration. In the present work, we have to consider two distinct cases, corresponding to the cluster and LMC field as previously defined. This section deals with the field only.

The LMC field is expected to follow a marked age-metallicity relation (AMR). This AMR has been measured by several authors using both field stars and star clusters of several ages (Mackey & Gilmore 2003; Kerber et al. 2007; Grocholski et al. 2006, 2007). In addition to the mean AMR, it is reasonable to expect a modest spread in metallicity at any given age. For this work, we adopt the scheme set by Kerber et al. (2009), in which we build partial models at 5 different metallicities disposed around the mean AMR of the LMC. Each partial model covers a range in logarithm of age of width 0.2 dex. For stellar populations younger than 10^8 yr, the numbers of observed stars are very small and hence we assume broader age bins, of widths 0.3 dex for $7.2 \leqslant \log(t/{\rm yr}) \leqslant 8.0$, together with a single age bin of width 0.8 dex for $\log(t/{\rm yr}) < 7.2$. The [Fe/H] separation between partial models is of 0.1 dex.

For the initial mass function (IMF) we adopt the

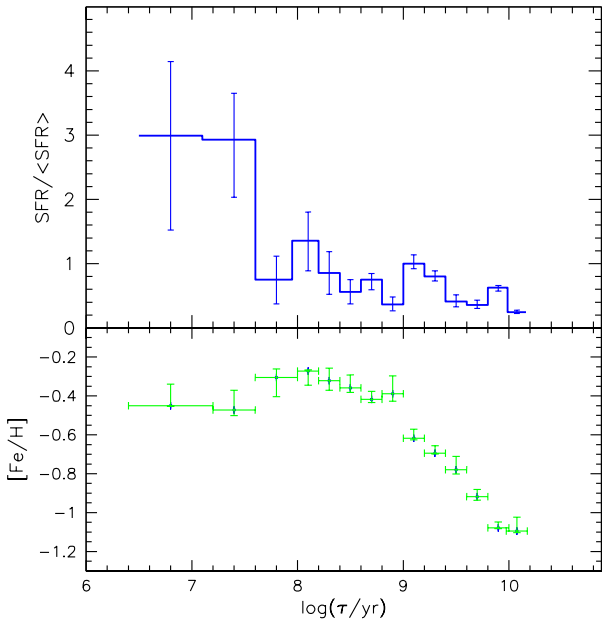


Figure 8. Top panel: best-fitting SFH for the field, together with the random errors (1σ). Bottom panel: the mean age–metallicity relation.

Chabrier (2001) one. The binary fraction is set to a value of 0.3 for binaries with mass ratios in the range between 0.7 and 1.0, which is consistent with the prescriptions for binaries commonly used in works devoted to recover the field SFH in the Magellanic Clouds (e.g. Holtzman et al. 1999; Harris & Zaritsky 2001; Javiel et al. 2005; Noël et al. 2009). Notice that this assumption is also in agreement with the few determinations of binary fraction for stellar clusters in the LMC (Elson et al. 1998a; Hu et al. 2008, both for NGC 1818, a stellar cluster younger than ~ 100 Myr).

3.2 The best-fitting solution

Once the database of partial models is built, we run StarFISH to find the best-fitting solution to the observed CMDs, for a given value of distance modulus $(m-M)_0$ and extinction A_V. Both F814W $\times$ F435W $-$ F814W and F814W $\times$ F555W $-$ F814W Hess diagrams are used simultaneously in the process of χ^2 minimization.

$(m-M)_0$ and A_V are then varied over the possible range of values. The χ^2 map of Fig. 6 shows the results in the $(m-M)_0 \times A_V$ plane. The overall best-fitting solution, with a $\chi^2_{\rm min}$ of 1.6, is located at $(m-M)_0 = 18.50$ and $A_V = 0.525$. The 68 % confidence level for this solution spans a narrow range in distance and reddening, which is just $\Delta(m-M)_0 = 0.12$ mag and $\Delta A_V = 0.07$ mag wide.

Figure 7 compares the Hess diagrams of the field data (left panel) and its overall best-fitting model (right panel). It is evident that the solutions found by StarFISH reproduce well the observed CMD features but for the Poisson noise.

Finally, Fig. 8 presents the SFR(t) and age–metallicity relation (AMR) corresponding to this best-fitting solution. It is remarkable that the recovered SFR(t) presents features that are consistent with those commonly found in previous works, based on both HST data (Olsen 1999; Holtzman et al. 1999; Smecker-Hane et al. 2002; Javiel et al. 2005) and ground-based data (Harris & Zaritsky 2001, 2009). There is an initial burst of star formation followed by a quiescent period, with a marked and peaked star formation for ages younger than 4 Gyr ($\log(t/{\rm yr}) = 9.6$). In particular the peaks of star formation at approximately 1.5 Gyr ($\log(t/{\rm yr}) = 9.2$), 500 Myr ($\log(t/{\rm yr}) = 8.7$), 100 Myr ($\log(t/{\rm yr}) = 8.0$) and 10 Myr ($\log(t/{\rm yr}) = 7.0$) are in tight agreement with those found by Harris & Zaritsky (2009) for the global SFH of the LMC. Concerning the AMR, the result for the NGC 1751 field is consistent with those derived from the LMC stellar clusters (Kerber et al. 2007; Harris & Zaritsky 2009) and for the LMC field (Carrera et al. 2008).

4 THE SFH FOR NGC 1751

4.1 Overview of NGC 1751 parameters from literature

As for the LMC field, also for the NGC 1751 cluster we need a set of physical parameters to start with the SFH-recovery work. They are based on the following works:

The cluster metallicity as determined by the Ca II method is of [Fe/H] $= -0.44 \pm 0.05$ (Grocholski et al. 2006), which is a typical value for an intermediate-age LMC cluster ([Fe/H] $= -0.48 \pm 0.09$; Grocholski et al. 2006).

Milone et al. (2009) identified a double MSTO in the HST/ACS F435W vs. F435W $-$ F814W CMD for this cluster. Using isochrone fitting, they determined ages between 1.3 and 1.5 Gyr, a distance modulus of 18.45 mag, $E_{B-V} = 0.22$ ($A_V \simeq 0.70$), and a metallicity of $Z = 0.008$ ([Fe/H] $\simeq -0.38$).

Milone et al. (2009) also determine a binary fraction $f_{\rm b}$ of 0.13 ± 0.1 for mass ratios q larger than 0.6 in NGC 1751. Despite the small error bar quoted by them, their estimate is admitedly a preliminary one. The careful determination from Elson et al. (1998b) for the LMC cluster NGC 1818, finds $f_{\rm b}$ values varying from ~ 0.20 to ~ 0.35 as one goes from the cluster center to the outer parts. We adopt here the conservative value of $f_{\rm b} = 0.2$ for $q > 0.7$. Our previous results for NGC 419 (Rubele et al. 2010) indicate that the results of the SFH recovery do not depend significantly on the choice of binary fraction.

As for the extinction, the reddening maps from the Magellanic Clouds Photometric Survey (MCPS; Zaritsky et al. 2004) and Pejcha & Stanek (2009) provide discrepant values for the NGC 1751 direction. Within 3 arcmin from the cluster, MCPS gives $A_V = 0.47 \pm 0.34$ for hot stars, and $A_V = 0.59 \pm 0.39$ for cool stars. From the same dataset, Pessev et al. (2008) determined $A_V = 0.65 \pm 0.06$. Pejcha & Stanek (2009) instead find $\langle E_{V-I} \rangle = 0.150 \pm 0.293$ ($\langle A_V \rangle = 0.293 \pm 0.062$), although their value is based on just 5 stars within a $2^\circ \times 2^\circ$ area.

The distance modulus to the LMC disk in the NGC 1751 direction is of about 18.55 mag, as revealed by independent methods: van der Marel & Cioni (2001, AGB stars); Olsen & Salyk (2002, red clump stars); Nikolaev et al. (2004, Cepheid stars); Subramanian & Subramaniam (2010, RC stars from MCPS).

The above-mentioned works provide the initial guesses

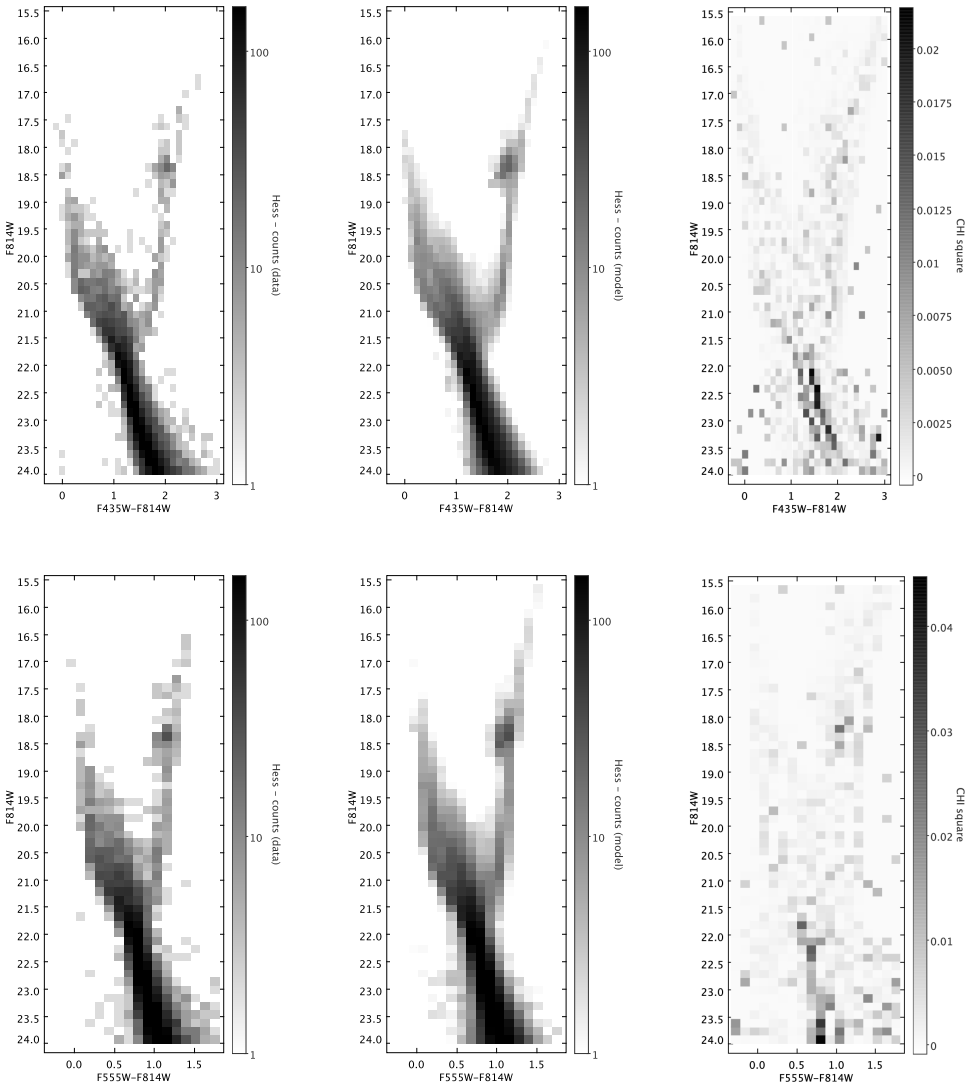


Figure 7. The Hess diagram for the NGC 1751 Field as derived from the ACS data (left panels), as recovered by the best-fitting solution (central panels), and the map of χ^2 residuals (right panels).

for the many cluster parameters to be determined in this work.

4.2 The partial models for NGC 1751

For NGC 1751 we assume a constant age-metallicity relation, i.e., a single value for the metallicity for all ages, since so far there are no evidences for significant spreads in metallicity in such star clusters (e.g. Mucciarelli et al. 2008; Rubele et al. 2010). The age interval covered by our partial models goes from $\log(t/\mathrm{yr}) = 8.9$ to 9.4, which is much wider than the interval suggested by the position of NGC 1751 MMSTOs. So, for each set of parameters, we have a total of 10 partial models, completely encompassing the age interval of interest. We have explored 5 metallicity values, going from [Fe/H] from -0.75 to -0.35 at steps of 0.1 dex. For each one of these mean [Fe/H] values, a small metallicity spread of 0.02 dex is assumed.

This definition of partial models might already be good enough to our aims to find the best-fitting solution for the cluster centre. However, we know that every portion of the ACS/WFC image is contaminated from the LMC field, and that this field contamination is well evident in the observed CMDs (especially for the Ring). Therefore, it is quite tempting to add, to the above-mentioned list of partial models, an additional one corresponding to the LMC field. The hope is that this partial model will allow StarFISH to properly fit the field contamination across the CMDs on NGC 1751, hence improving the fitting of cluster itself.

The inclusion of a partial model for the field is a novelty of this work, and is suggested as an alternative to the commonly used method of field star decontamination (see e.g., Milone et al. 2009; Bonatto & Bica 2007), which consists in subtracting from the cluster CMD the stars with colors and magnitudes similar to the ones in the field *before* deriving the cluster parameters. The advantage of our

method is that the field becomes an integral part of the χ^2 and error analysis; the latter is performed using the correct number statistics – i.e. considering the Poisson noise from the field, which is certainly present in cluster data – without implying any change in the method already set for these tasks.

There are then two different ways at which this partial model for the field can be built. (1) The simplest one is that of taking the observed Hess diagrams for the field region (left panels in Fig. 7). This diagram however is affected by the Poisson fluctuations in the numbers of stars, so that it might not describe in a suitable way the field actually observed in other parts of the ACS images. (2) The second alternative is to use the Hess diagram built from the best-fitting solution of the field (right panels in Fig. 7) which is obviously much more continuous and smooth over the CMDs than the observed one. This model has another clear advantage: the Hess diagram can be easily re-built using the output SFH for the field *together* with the ASTs derived for the cluster Centre or Ring. In this way, we are able to simulate the field under the same conditions of crowding met in the cluster data. We indeed adopt this latter alternative in the following.

4.3 The SFH for the cluster Centre

4.3.1 Results with and without the LMC field

The SFH-recovery is performed assuming a given set of $(m-M)_0$, A_V, and [Fe/H] values and fixing the binary fraction at a value of 0.2 in the case of cluster models. In order to limit the space of parameters to be covered, the procedure is essentially the following: for a given value of [Fe/H], we perform SFH-recovery for each point in a grid covering a significant region of the $(m-M)_0$ versus A_V plane, so as to build a map of the $\chi^2_{\rm min}$ for the solutions. Examples of these maps are presented in Fig. 9. The maps are extended enough so that the minimum $\chi^2_{\rm min}$ for a given value of [Fe/H] can be clearly identified, as well as the regions in which $\chi^2_{\rm min}$ increases by a factor of about 1.5. The typical resolution of such maps is of 0.02 mag in $(m-M)_0$ and 0.02 mag in A_V.

Let us first start discussing the case of the cluster Centre. Fig. 10 shows the maps of $\chi^2_{\rm min}$ as a function of $(m-M)_0$ and A_V, for two series of SFH-recovery experiments made under very similar conditions, i.e. using the same data and ASTs. The only difference is that in some cases (hereafter **case A**), we do not use the partial model for the LMC field in StarFISH, whereas in other cases we do it (hereafter **case B**). The result of considering the LMC field is quite evident: although in both A and B cases the best-fitting solution is found for about the same value of $(m-M)_0$ and A_V, in case B the $\chi^2_{\rm min}$ values are systematically smaller, which means better overall fits of the CMDs. Moreover, it is evident that in case A the presence of the LMC field falses the determination of the best-fitting cluster metallicity: indeed, in case A the best-fitting model of [Fe/H] $= -0.64$ is found to be slightly favoured over the one with [Fe/H] $= -0.44$. In case B, instead, the best-fitting solution at [Fe/H] $= -0.44$ is clearly favoured. Notice that, at the ~ 1.5 Gyr old ages of NGC 1751, the field is found to have a metallicity of about -0.65 (see Fig. 8), which probably helps, in case A, to move the $\chi^2_{\rm min}$ minimum to [Fe/H] $= -0.64$.

These experiments demonstrate that even a small fraction of field contamination may affect significantly the results of SFH-recovery, if not properly taken into account. In the following, we adopt case B as the default, since it demonstrately takes the LMC field into account and improves the quality of the final results for the Centre of NGC 1751.

4.3.2 Characteristics of the best-fitting solution

Complete maps of $\chi^2_{\rm min}$ for the Centre, as a function of $(m-M)_0$, A_V and metallicity, are presented in the left panels of Fig. 9. It may be noticed that the best solution is indeed for [Fe/H] $= -0.44$, $(m-M)_0 = 18.58$, and $A_V = 0.50$, with a $\chi^2_{\rm min} = 0.62$. Such a small $\chi^2_{\rm min}$ is already an indication of an excellent fit to the observational data.

This best-fitting solution and map of residuals are also presented in the Hess diagrams of Fig. 11. Finally, the best-fitting solution for the cluster Centre is in the left panel of Fig. 12.

4.3.3 Evaluating the errors

To evaluate the errors for all involved parameters, the first step is to find the correspondence between the $\chi^2_{\rm min}$ value for each model and its significance (or confidence) level, α. This correspondence was estimated simulating 100 synthetic CMDs generated with a number of stars equal to the observed CMD, using the best-fitting SFR(t) and its parameters as the input for the simulations. So, after recovering the SFH for this sample of synthetic CMDs, it was possible to build the $\chi^2_{\rm min}$ distribution and to establish the relation between the $\chi^2_{\rm min}$ difference above the minimum and α.

In the $\chi^2_{\rm min}$ maps of Fig. 9, we superimposed the 68 % and 95 % significance levels for all the solutions for the centre. Only for the [Fe/H] $= -0.44$ map we find ample areas of the A_V versus $(m-M)_0$ diagram with solutions within the 68 % significance level of the best solution. Based on this figure, we determine $(m-M)_0 = 18.58 \pm 0.07$ and $A_V = 0.50 \pm 0.05$ for the cluster Centre (with random errors at the 68 % significance level).

The left panel of Fig. 12 shows the SFR(t) for the cluster Centre together with error bars. The most basic feature in this plot is that the SFR(t) is clearly non-null for three age bins, spanning the $\log(t/{\rm yr})$ interval from 9.05 to 9.2 (ages from 1.12 to 1.58 Gyr). Note that this result is not only valid for the best fitting model, but also across the entire 68 % significance level area of the A_V versus $(m-M)_0$ diagram. Moreover, it is non-null even in the case we adopt more restrictive limits for the random errors, i.e. if we plot the random errors for the 95 % significance level.

Then, one may wonder how the solution for the Centre changes if we adopt a better age resolution in the SFH-recovery. This is shown in Fig. 13, where we compare the solution for $\Delta\log({\rm age}) = 0.05$ dex with the one obtained with the same data and methods, but for an age resolution of $\Delta\log({\rm age}) = 0.025$ dex. As we see, within the error bars the two solutions are essentially the same. The finer resolution in age is compensated by an increase in random errors.

Therefore, we find evidence that in the NGC 1751 Centre the SFR(t) has lasted for a timespan of 460 Myr. This is about twice longer than the $\sim$ 200 Myr estimated by

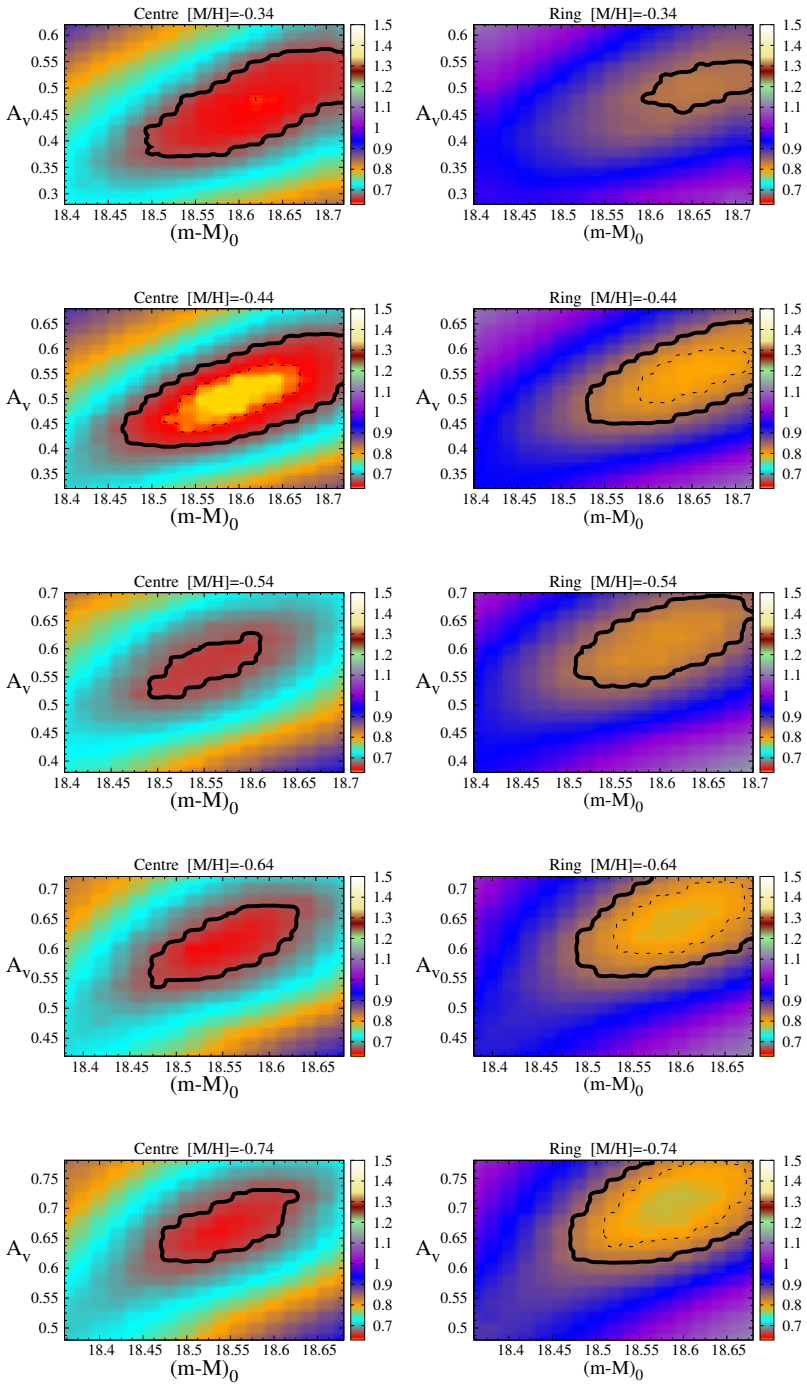


Figure 9. Maps of the $\chi^2_{\rm min}$ obtained from the SFH-recovery, as a function of $(m-M)_0$ and A_V, for several [Fe/H] values (from -0.34 to -0.74 at steps of -0.1 dex, from top to bottom) and for both the cluster Centre and Ring (left and righ panels, respectively). The black lines delimit the regions within a 68 % (continuous line) and 95 % confidence levels (dotted lines) of the absolute best solution, which is found at -0.34 dex for the Centre, and at -0.74 dex for the Ring. The $\chi^2_{\rm min}$ for the Centre best solution is of 0.625.

Milone et al. (2009) for the same cluster, based on a simple comparison with the MSTO locations of different isochrones.

4.4 The SFH for the cluster Ring

We have performed the same experiments of SFH-recovery separately for the Ring, as illustrated in the $\chi^2_{\rm min}$ maps at the central and right panels of Fig. 9. In these cases, the levels of $\chi^2_{\rm min}$ are significantly higher than for the cluster Centre. This result may seem surprising, considering that the Ring has a lower level of crowding and hence deeper photometry than the Centre. We consider as unlikely that these higher $\chi^2_{\rm min}$ for the Ring could be simply caused by its higher level of contamination from the LMC field, since

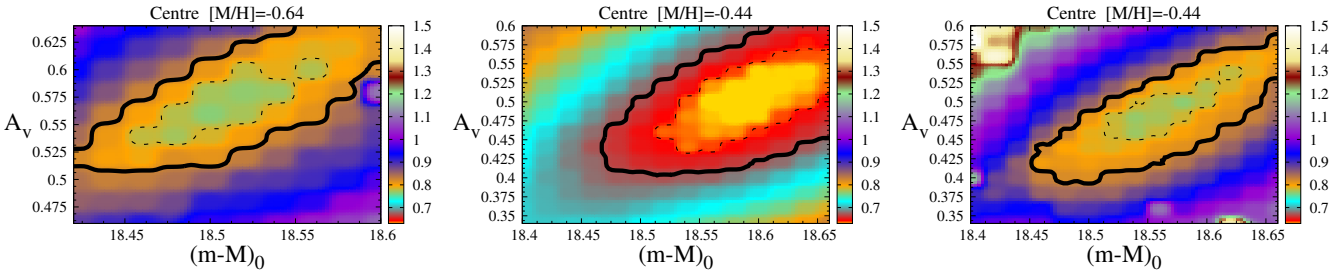


Figure 10. Maps of the $\chi^2_{\rm min}$ obtained during SFH-recovery in the Centre region, as a function of $(m-M)_0$ and A_V. The **left panel** shows the map for the best-fitting metallicity of [Fe/H] $= -0.64$, obtained in the case A (i.e. not taking into account a partial model for the LMC field). The minimum $\chi^2_{\rm min}$ is of 0.77. The **middle panel** shows the same for case B (i.e. using the LMC field partial model) and [Fe/H] $= -0.44$, which is the best-fitting metallicity in this case. It is evident that these solutions are characterized by a significantly smaller level of $\chi^2_{\rm min}$ overall, with a minimum at 0.62. For comparison, the **right panel** shows the best-fitting solutions for case A and [Fe/H] $= -0.44$. Also in this case, the $\chi^2_{\rm min}$ are significantly higher (and very close to the one in the letfmost panel).

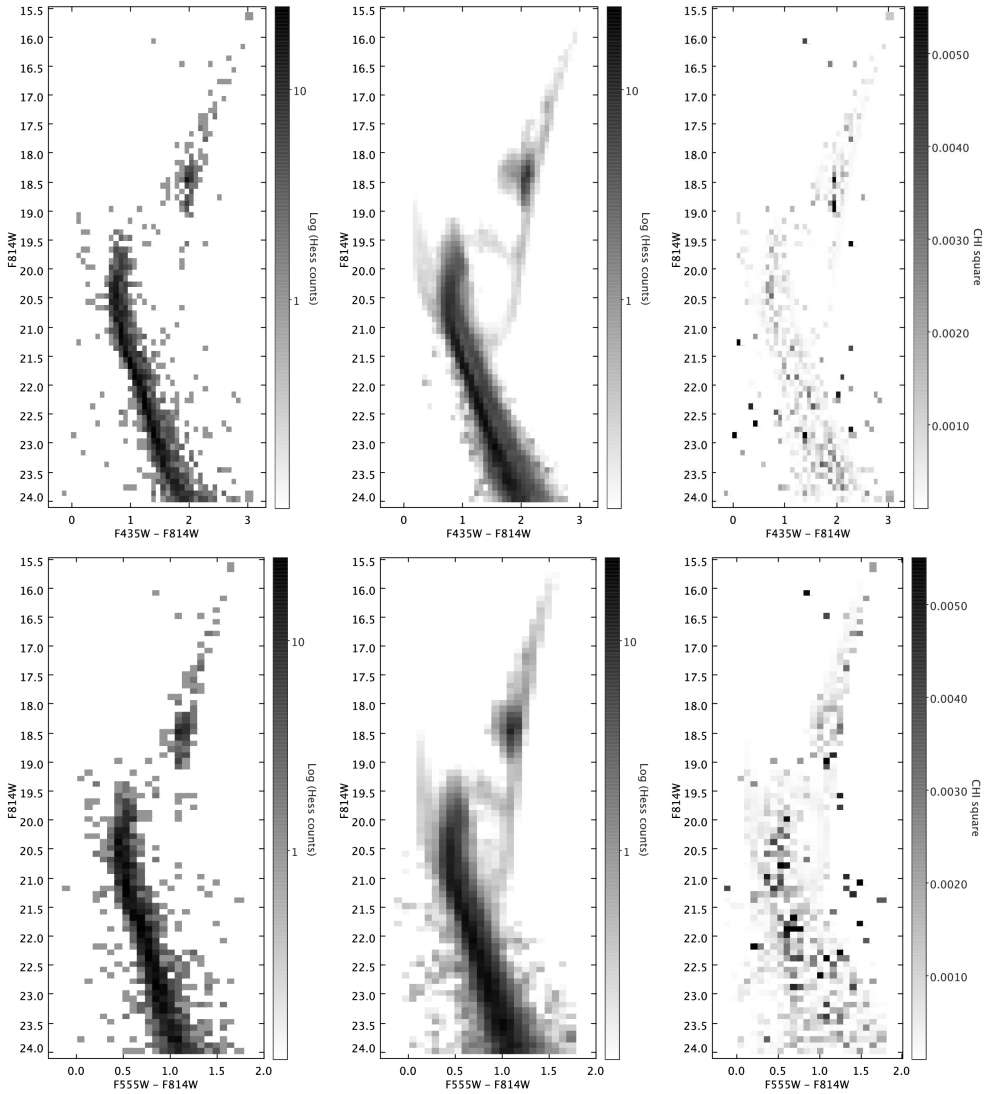


Figure 11. The Hess diagrams for the NGC 1751 Centre data (left panels), its best-fitting solution model (central panels), and the χ^2 map (right panels). The top panels are for the F435W $-$ F814W vs. F814W diagrams, the bottom ones for F555W $-$ F814W vs. F814W.

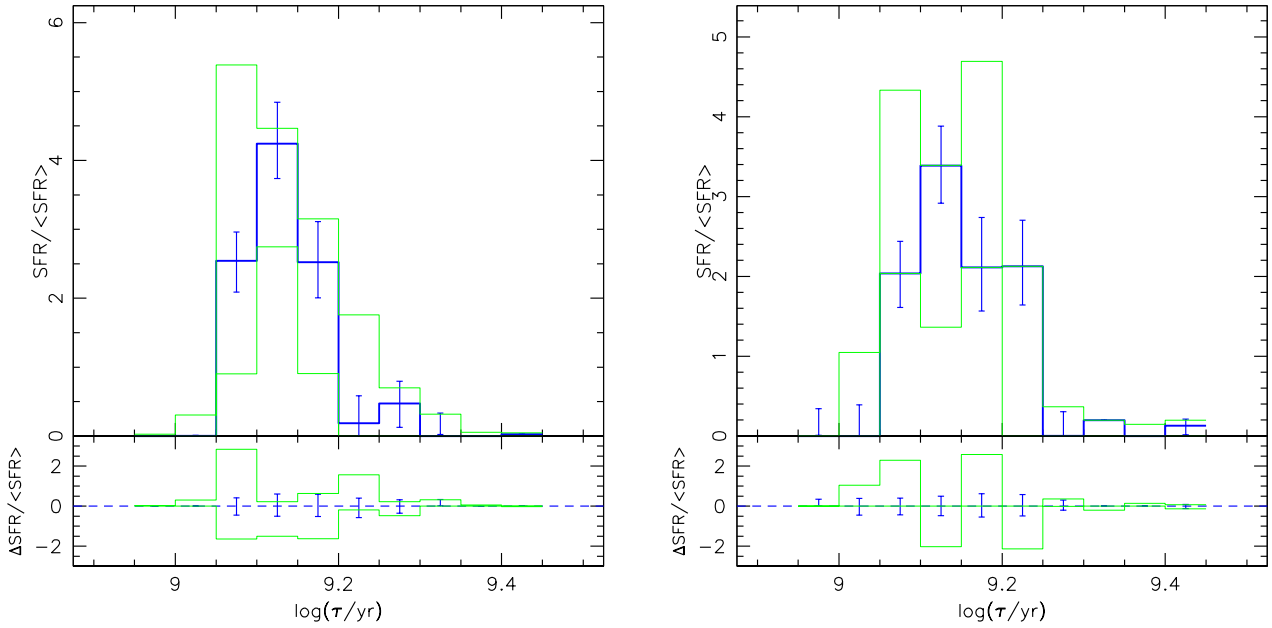


Figure 12. The blue lines show the SFR(t) for the cluster Centre (left panel) and for the Ring (right panel). The error bars are random errors. The green lines indicate the systematic errors, inside the area of 68 % confidence level in Fig. 9.

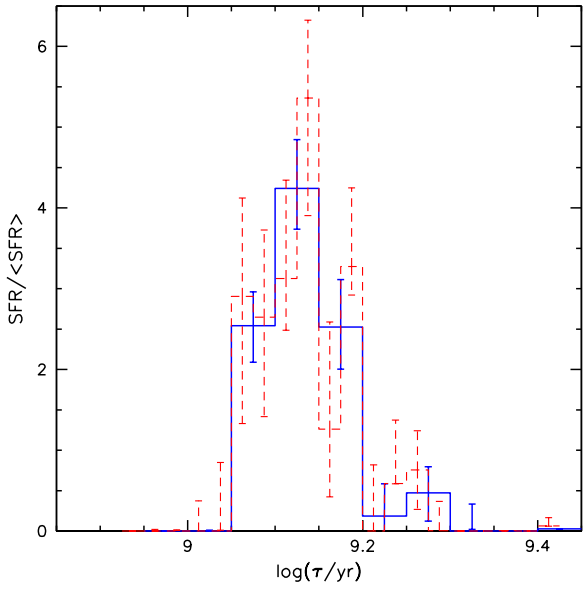


Figure 13. Comparison between the SFR(t) for two best-fitting solutions for the cluster Centre, obtained with different age resolutions: with $\Delta \log t = 0.050$ dex (blue continuous line) and with $\Delta \log t = 0.025$ dex (red dashed line).

this field is very well modeled anyway, and fully taken into account in the SFH recovery.

Instead, the main reason for the worst fits could be on the presence of a differential reddening of about $E_{B-V} \sim 0.10$ mag within the ACS field, as found by Milone et al. (2009) and Goudfrooij et al. (in preparation).

To test for the presence of differential reddening we have followed a similar procedure as described by Milone et al. (2009), following the position of fiducial lines in the F435W − F555W vs. F555W − F814W diagram, and as illustrated in Fig. 14. So by means of the relative shifts in the fiducial lines in this colour-colour diagram along the reddening arrow we have found an extra reddening in the Ring region in relation to the Centre, with a magnitude in $E_{\rm F555W-F814W}$ similar to the one presented by Milone et al. (2009). This extra reddening occurs prevalently in the bottom and upper extremities of the Ring in Fig. 1.

Notice also that the extinction values for the Ring, found during the experiments of SFH-recovery are systematically higher than the ones found for the Centre region (see Fig. 9), which independently confirms the presence of differential reddening detected by us and Milone et al. (2009) using fiducial lines.

Unfortunately the recovered best-fitting $(m-M)_0$ and [Fe/H] values for the Ring are obviously spurious, since they are not consistent with the ones found for the Centre – which is a such small region that one can consider it free from differential reddening. Considering the high quality of the SFH-recovery for the cluster Centre (as demonstrated by the much smaller $\chi^2_{\rm min}$), we assume that the correct distance and reddening of the Ring are the same ones as for the Centre, namely $(m-M)_0 = 18.58$ and $A_V = 0.50$. The right panel of Fig. 12 shows the Ring SFH for these parameters.

It is interesting to note that the Ring SFR(t), considering just the random errors, seems to be slightly more spread in age than the one for the Centre. Indeed, the SFR(t) is found to be non-null in an additional, older age bin, as compared to the cluster Centre. However, when one considers the systematics errors in this bin, it is clear that this result is not solid. It becomes then impossible to take any conclusion in relation to a possible dependence of the SFR(t) with the cluster radius.

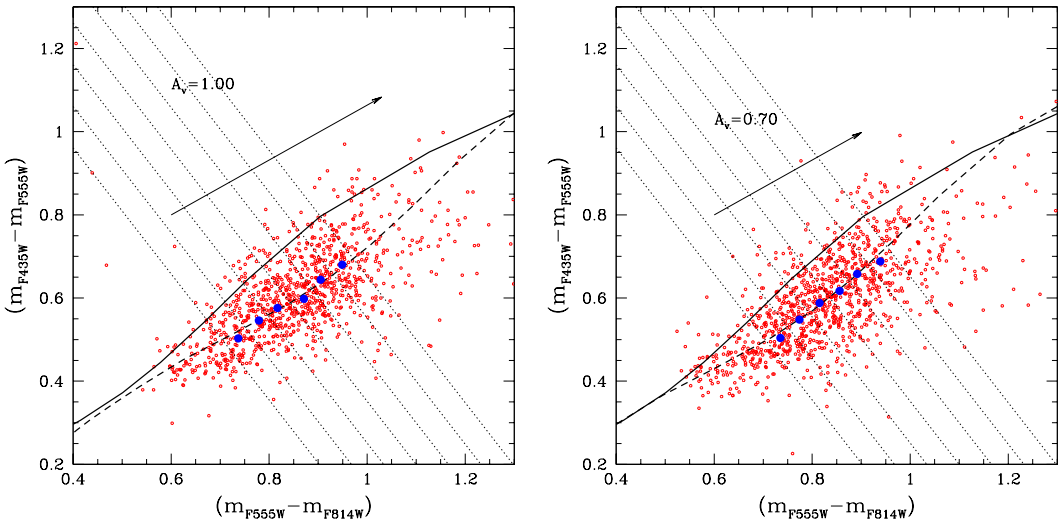


Figure 14. Colour-colour diagrams for the northern (left panel) and southern (right panel) half-sections of the Ring, illustrating the method used to determine the presence of differential reddening. Only the data for the lower main sequence, with F814W between 21.5 and 23.5, is plotted (red dots). The blue dots mark the median position of the observed stars in small colour bins (dotted lines) perpendicular to the reddened main sequence. The continuous dark line is an unreddened model zero-age main sequence. The dashed line shows the position of the reddened main sequence that best fit these blue dots. Although the reddening vector (arrow) runs almost parallel to the main sequence, it is clear that the median position of the points in this plot can be used to derive the mean reddening in a field. We do it differentially, determining that between the northern and southern sections of the Ring there is a difference in A_V of 0.30 mag, which corresponds to 0.10 mag in E_{B-V}.

5 CONCLUDING REMARKS

In this work, we confirm that NGC 1751 hosts a dual red clump, similar to the one observed in the SMC cluster NGC 419 (Girardi et al. 2009). Then, we perform SFH-recovery via the classical method of CMD reconstruction with the sum of single-burst stellar populations. The basic result is that in the NGC 1751 Centre star formation is found to last for a timespan of 460 Myr. The same result is consistently found irrespective of the method used to take field contamination into account, of the age resolution adopted, and for a significant region of the A_V versus $(m-M)_0$ plane. The age resolution of the method is at least 3 times smaller than this interval. In addition, the best-fitting model is indeed a quite good representation of the observed data. On the other hand, the CMD for the cluster Centre is so obviously sharp and clean from the LMC field, that it is hard to imagine that some important effect has not been properly considered in our analysis.

Our results contrast with those obtained by Milone et al. (2009), who identify just two episodes of star formation separated by 200 Myr in this cluster, using the method of isochrone fitting.

For the cluster Ring, the results indicate a SFR timespan of at least 460 Myr, with a significantly lower quality of the results, as indicated by the larger $\chi^2_{\rm min}$ and by the best fitting model being found for a distance different from the cluster Centre. These failures probably depend on the presence of significant differential reddening across the Ring. So, we prefer not to take any conclusion from this region. Unfortunately, our method finishes in not providing any indication about possible variations in the spatial distribution of the stars with different ages, which would be important for the goals of understanding the mechanism of extended star formation (see Goudfrooij et al. 2009).

Together with our previous findings for NGC 419 (Rubele et al. 2010), the results for the NGC 1751 Centre argue in favour of multiple star formation episodes (or continued star formation) being at the origin of the MMSTOs in Magellanic Cloud clusters with ages around 1.5 Gyr. The hypothesis of a spread caused by the presence of fast rotators among the upper main sequence stars (Bastian & de Mink 2009) is separately discussed by Girardi, Eggenberger, & Miglio (2011), who conclude that it does not offer a valid alternative to the conclusions reached in the present paper.

ACKNOWLEDGMENTS

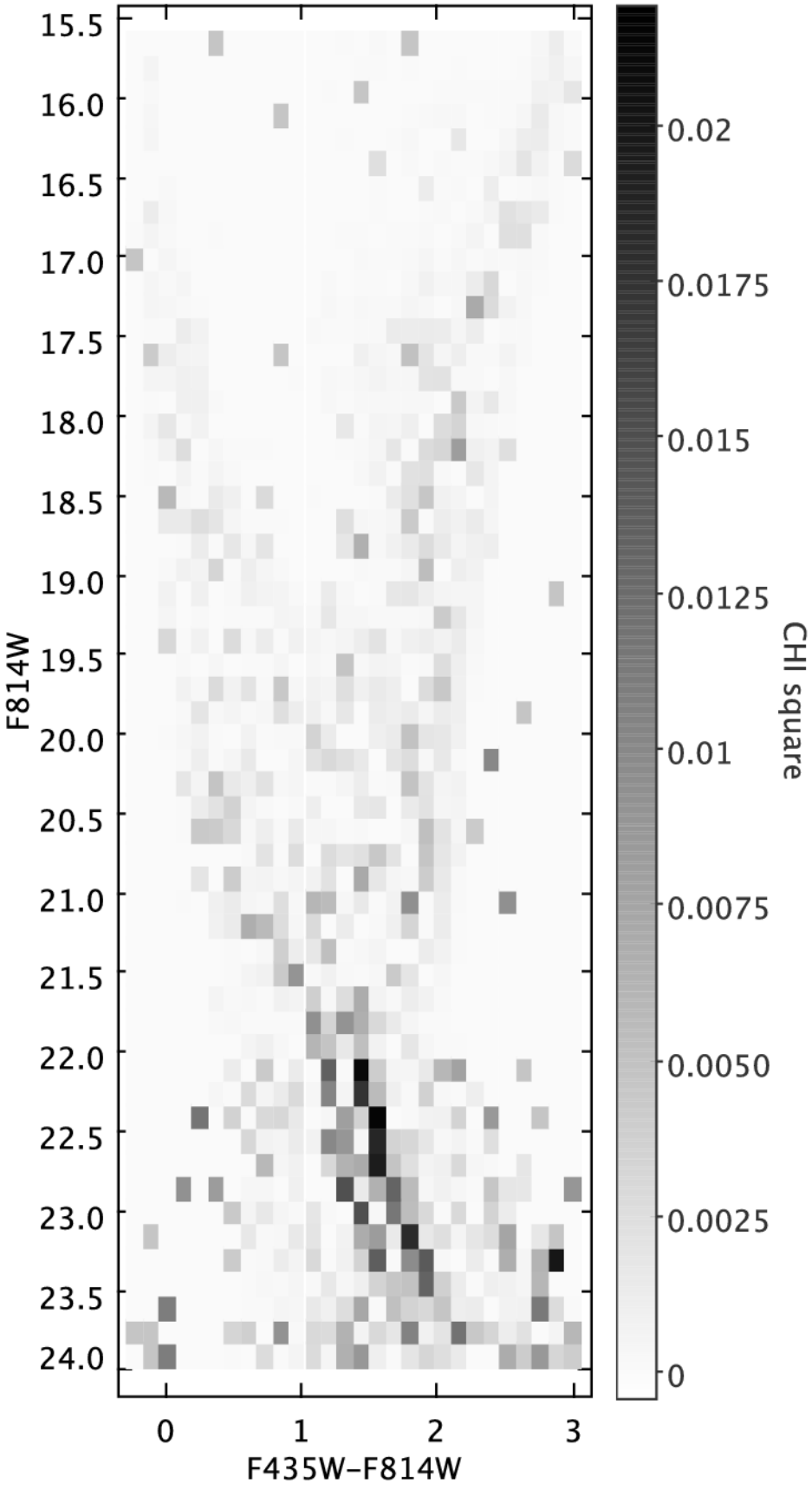
We thank the anonymous referee for the useful suggestions. VKP is grateful to Jay Anderson for sharing his ePSF program.

The data presented in this paper were obtained from the Multimission Archive at the Space Telescope Science Institute (MAST). STScI is operated by the Association of Universities for Research in Astronomy, Inc., under NASA contract NAS5-26555. We thank the support from INAF/PRIN07 CRA 1.06.10.03, contracts ASI-INAF I/016/07/0 and ASI-INAF I/009/10/0, and the Brazilian agencies CNPq and FAPESP.

REFERENCES

Bastian N., de Mink S. E., 2009, MNRAS, 398, L11
Bonatto C., Bica E., 2007, MNRAS, 377, 1301

Bressan A. G., Chiosi C., Bertelli G., 1981, A&A, 102, 25
Carrera R., Gallart C., Hardy E., Aparicio A., Zinn R., 2008, AJ, 135, 836
Chabrier G., 2001, ApJ, 554, 1274
Cioni M., et al. 2011, A&A, in press, arXiv:1012.5193
Dolphin A. E., 2002, MNRAS, 332, 91
Elson R. A. W., Sigurdsson S., Davies M., Hurley J., Gilmore G., 1998a, MNRAS, 300, 857
Elson R. A. W., Sigurdsson S., Davies M., Hurley J., Gilmore G., 1998b, MNRAS, 300, 857
Gallart C., Freedman W. L., Aparicio A., Bertelli G., Chiosi C., 1999, AJ, 118, 2245
Girardi L., 1999, MNRAS, 308, 818
Girardi L., Bressan A., Bertelli G., Chiosi C., 2000, A&AS, 141, 371
Girardi L., Rubele S., Kerber L., 2009, MNRAS, 394, L74
Girardi L., Rubele S., Kerber L., 2010, in R. de Grijs & J. R. D. Lépine ed., IAU Symposium Vol. 266 of IAU Symposium, Star clusters with dual red clumps. pp 320–325
Girardi L., Eggenberger P., Miglio A., 2011, MNRAS, L204
Glatt K., Grebel E. K., Sabbi E., Gallagher J. S., Nota A., Sirianni M., Clementini G., Tosi M., Harbeck D., Koch A., Kayser A., Da Costa G., 2008, AJ, 136, 1703
Goudfrooij P., Puzia T. H., Kozhurina-Platais V., Chandar R., 2009, AJ, 137, 4988
Grocholski A. J., Cole A. A., Sarajedini A., Geisler D., Smith V. V., 2006, AJ, 132, 1630
Grocholski A. J., Sarajedini A., Olsen K. A. G., Tiede G. P., Mancone C. L., 2007, AJ, 134, 680
Harris J., Zaritsky D., 2001, ApJS, 136, 25
Harris J., Zaritsky D., 2004, AJ, 127, 1531
Harris J., Zaritsky D., 2009, AJ, 138, 1243
Holtzman J. A., Gallagher III J. S., Cole A. A., Mould J. R., Grillmair C. J., Ballester G. E., Burrows C. J., Clarke J. T., Crisp D., Evans R. W., Griffiths R. E., Hester J. J., Hoessel J. G., Scowen P. A., Stapelfeldt K. R., Trauger J. T., Watson A. M., 1999, AJ, 118, 2262
Hu Y., Deng L., deGrijs R., Goodwin S. P., Liu Q., 2008, ArXiv e-prints, 801
Javiel S. C., Santiago B. X., Kerber L. O., 2005, A&A, 431, 73
Kerber L. O., Girardi L., Rubele S., Cioni M.-R., 2009, A&A, 499, 697
Kerber L. O., Santiago B. X., Brocato E., 2007, A&A, 462, 139
Mackey A. D., Broby Nielsen P., 2007, MNRAS, 379, 151
Mackey A. D., Broby Nielsen P., Ferguson A. M. N., Richardson J. C., 2008, ApJ, 681, L17
Mackey A. D., Gilmore G. F., 2003, MNRAS, 338, 85
Milone A. P., Bedin L. R., Piotto G., Anderson J., 2009, A&A, 497, 755
Mucciarelli A., Carretta E., Origlia L., Ferraro F. R., 2008, AJ, 136, 375
Nikolaev S., Drake A. J., Keller S. C., Cook K. H., Dalal N., Griest K., Welch D. L., Kanbur S. M., 2004, ApJ, 601, 260
Noël N. E. D., Aparicio A., Gallart C., Hidalgo S. L., Costa E., Méndez R. A., 2009, ApJ, 705, 1260
Olsen K. A. G., 1999, AJ, 117, 2244
Olsen K. A. G., Salyk C., 2002, AJ, 124, 2045
Pejcha O., Stanek K. Z., 2009, ApJ, 704, 1730
Pessev P. M., Goudfrooij P., Puzia T. H., Chandar R., 2008, MNRAS, 385, 1535
Piatti A. E., Geisler D., Bica E., Clariá J. J., Santos J. F. C., Jr., Sarajedini A., Dottori H., 1999, AJ, 118, 2865
Riess A., Mack J., 2004, Technical report, Time Dependence of ACS WFC CTE Corrections for Photometry and Future Predictions. Space Telescope Science Institute
Rubele S., Kerber L., Girardi L., 2010, MNRAS, 403, 1156
Smecker-Hane T. A., Cole A. A., Gallagher III J. S., Stetson P. B., 2002, ApJ, 566, 239
Subramanian S., Subramaniam A., 2010, A&A, 520, 24
van der Marel R. P., Cioni M.-R. L., 2001, AJ, 122, 1807
Zaritsky D., Harris J., Thompson I. B., Grebel E. K., 2004, AJ, 128, 1606


15.5
16.0
16.5
17.0
17.5
18.0
18.5
19.0
19.5
20.0
20.5
21.0
21.5
22.0
22.5
23.0
23.5
24.0
F814W
0
1
2
3
F435W-F814W
0.02
0.0175
0.015
0.0125
0.01
0.0075
0.0050
0.0025
0
CHI square